ACS Synthetic Biology

Letter

pubs.acs.org/synthbio

An Orthogonal Multi-input Integration System to Control Gene Expression in *Escherichia coli*

Fabio Annunziata,[#,†,⊥] Antoni Matyjaszkiewicz,[#,‡,⊥] Gianfranco Fiore,[‡,⊥] Claire S. Grierson,[§,⊥] Lucia Marucci,[‡,⊥] Mario di Bernardo,[*,#,‡,∥,⊥] and Nigel J. Savery[*,#,†,⊥]

[†]School of Biochemistry, University of Bristol, BS8 1TD, Bristol, U.K.

[‡]Department of Engineering Mathematics, University of Bristol, BS8 1UB, Bristol, U.K.

[§]School of Biological Sciences, University of Bristol, BS8 1UH, Bristol, U.K.

[∥]Department of Electrical Engineering and Information Technology, University of Naples Federico II, 80125, Naples, Italy

[⊥]BrisSynBio, Bristol, BS8 1TQ, U.K.

Supporting Information

ABSTRACT: In many biotechnological applications, it is useful for gene expression to be regulated by multiple signals, as this allows the programming of complex behavior. Here we implement, in *Escherichia coli*, a system that compares the concentration of two signal molecules, and tunes GFP expression proportionally to their relative abundance. The computation is performed *via* molecular titration between an orthogonal σ factor and its cognate anti-σ factor. We use mathematical modeling and experiments to show that the computation system is predictable and able to adapt GFP expression dynamically to a wide range of combinations of the two signals, and our model qualitatively captures most of these behaviors. We also demonstrate *in silico* the practical applicability of the system as a reference-comparator, which compares an intrinsic signal (reflecting the state of the system) with an extrinsic signal (reflecting the desired reference state) in a multicellular feedback control strategy.

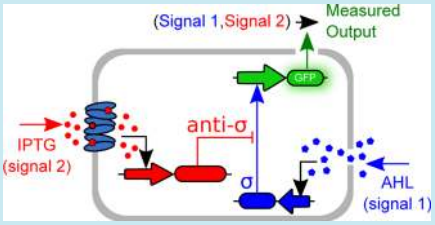

The ability to program and control information processing functions in living cells is of great interest for biotechnological and synthetic biology applications. In many such applications it is useful to be able to compare the state of the system with some reference state signal. For example, to coordinate the production phase with a specific growth or environmental condition during industrial fermentation,[1,2] or to compare a proxy for population density with a specific external signal to trigger the release of a defined metabolite during biosensing and bioactuation, (*e.g.*, antibiotic[3,4]). Many attempts have been made to reconstitute fundamental molecular pathways and modules for signal integration and information processing.[5−11] These approaches rely on molecular interactions between proteins, DNA and RNA, and have been useful to design and implement genetic components that integrate multiple signals to activate or repress gene expression. Unfortunately these often have predetermined outcomes, and cannot dynamically adapt their activation thresholds in response to signal profiles that change over time. Such an ability is fundamental for living cells to perform fast adaptation and development, in the context of rapidly changing external and internal cues.

Protein−protein interaction and sequestration have been proposed, and partially experimentally validated, as a good mechanism for the construction of adaptable synthetic pathways.[12−14] In a validation of protein sequestration mechanisms for genetic networks, Buchler and Cross showed that protein sequestration by dominant negative inhibitors is able to generate ultrasensitive responses that can be used to easily tune the response of a genetic circuit.[12] Furthermore, protein sequestration connected to positive feedback loops has been used to fine-tune the behavior of genetic switches in a synthetic network.[13] However, protein sequestration was achieved by protein swapping from a three-element protein complex, thus making the system cumbersome to integrate in larger synthetic networks. It has also been shown that that protein sequestration can be used to generate a signal tracking circuit, where the expression of an antiscaffold protein (acting as an inhibitor of a protein complex formation and used as reference signal tracking system) can be linked *via* negative feedback loops to the expression level of a transcriptional activator (acting as the output of the system).[14] The proposed circuit is able to track only one external signal, linking it to internal processes (*e.g.*, expression levels) and making it unsuitable for multisignal integration and real-time external signal processing.

In their pioneering work, Rhodius *et al.*[15] described a threshold activated gate based on sequestration of the σ subunit of RNA polymerase by a cognate anti-σ factor, proving that molecular titration can regulate gene expression in response to compared inducer concentrations, without additional genetic manipulation.

Received: April 3, 2017
Published: July 19, 2017

DOI: 10.1021/acssynbio.7b00109
ACS Synth. Biol. XXXX, XXX, XXX−XXX

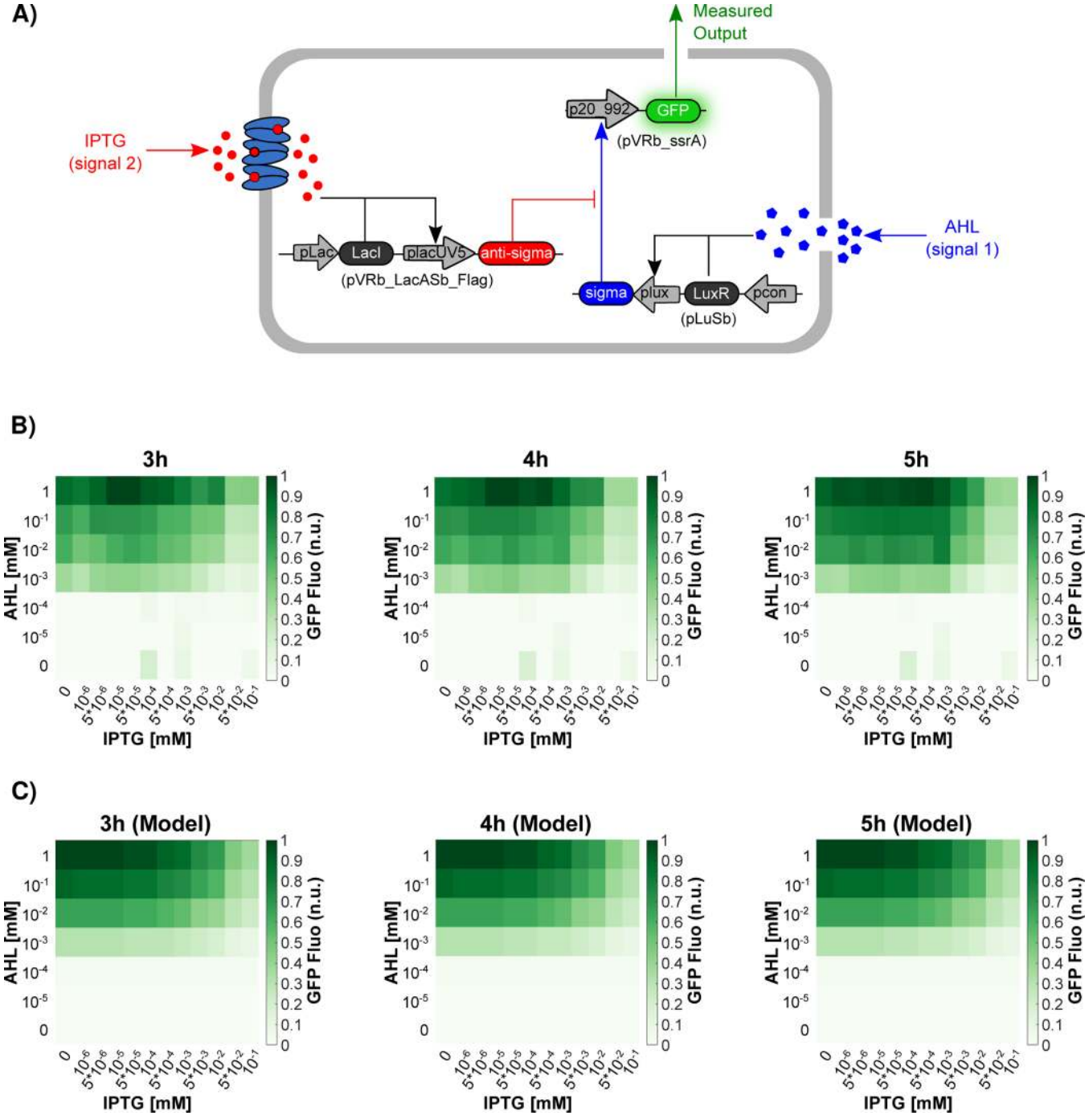

Figure 1. GFP expression is adapted to the computation of a wide range of signal intensities. (A) The proposed signal computation system. pcon indicates an *E. coli* constitutive promoter. (B) GFP expression profile at the indicated time points post-treatment with the indicated concentrations of AHL and IPTG. Data are averages of three independent experiments. (C) Mathematical simulations of the computation system at indicated time points after treatment with the indicated concentration of AHL and IPTG. (B–C) GFP values are shown as heatmaps of scaled values across the entire dynamical range of expression levels.

Here we present an in-depth analysis of the tunability and sensitivity of a σ/anti-σ module derived from the work of Rhodius *et al.*,[15] including its dynamic characterization, and its ability to efficiently compare different signal intensities and generate designed expression patterns. We also derive a detailed mathematical model of the module, able to capture most of the qualitative behavior observed experimentally. The goal is to propose a simple yet effective protein–protein sequestration module that is easier to embed in larger synthetic networks and that can be used to perform multisignal integration.

The system relies on protein/protein titration to compute the relative amounts of the quorum sensing molecule 3-O-C_6-HSL (AHL) and the chemical activator Isopropyl β-D-1-thiogalacto-pyranoside (IPTG), and tune the expression of a Green Fluorescent Protein (GFP) proportionally to the excess of AHL over IPTG. At the molecular level, the computation of the two signals and the tunable induction of GFP expression is

DOI: 10.1021/acssynbio.7b00109
ACS Synth. Biol. XXXX, XXX, XXX–XXX

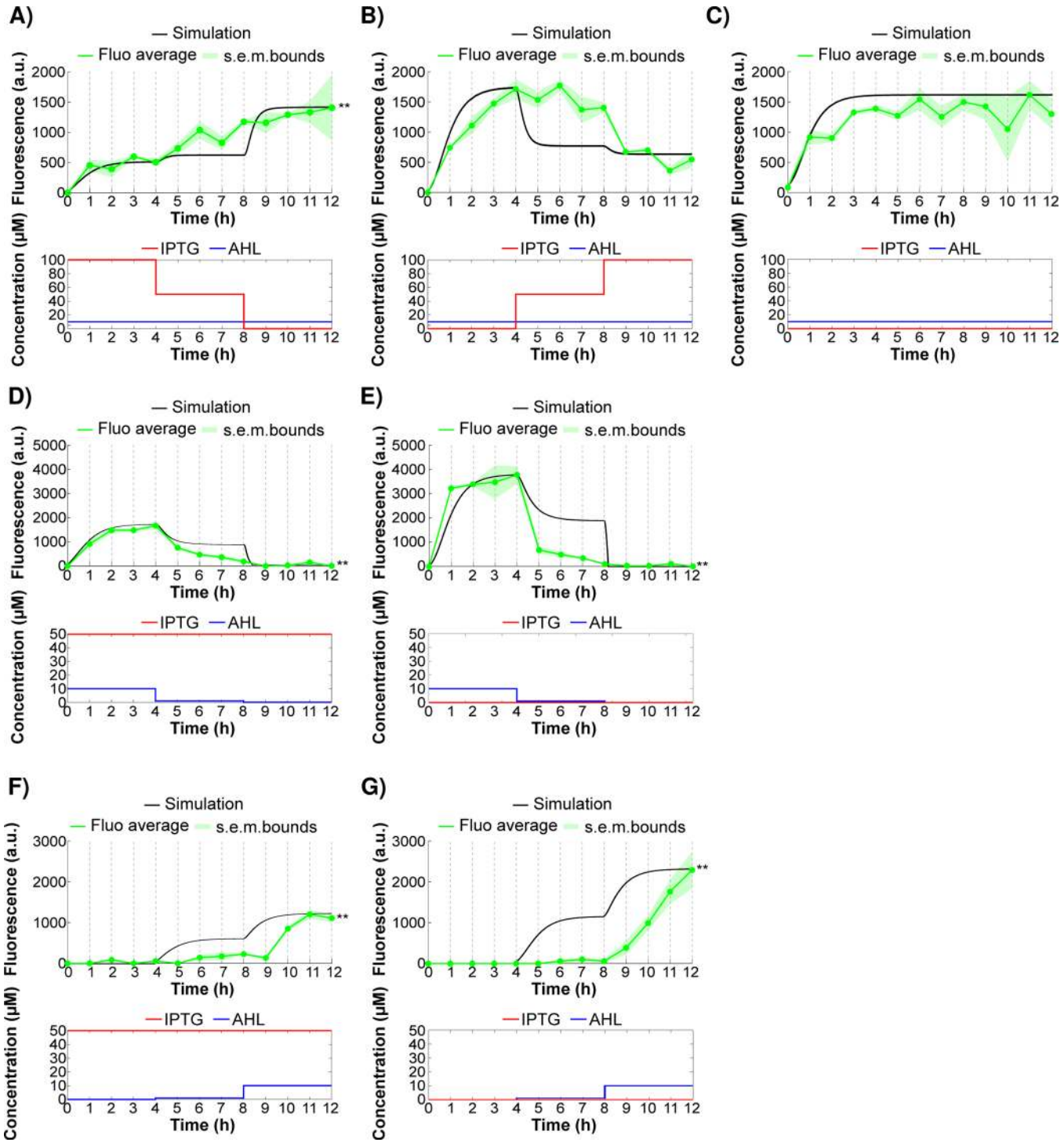

Figure 2. Signal computation is achieved with time-varying inducer concentrations. (A–G) Mathematical simulations (black lines) and measured GFP expression profiles (green line) at the indicated combination of AHL and IPTG concentrations. GFP fluorescence was measured and cells diluted every hour (dashed gray lines). Data are averages of three independent experiments and s.e.m. is shown as shadowed green area. (A,B,D,E,F,G) Spearman's correlation coefficient (r) and p-value (p) for the entire time course: (A) $r_s = 0.920$; $p = 0.0004$; (B) $r_s = 0.352$; $p = 0.238$; (D) $r_s = 0.725$; $p = 0.005$; (E) $r_s = 0.701$; $p = 0.008$; (F) $r_s = 0.793$; $p = 0.001$ (G) $r_s = 0.923$; $p = 0.000007$. * Significant correlation ($0.6 < r_s < 1$) at the 0.05 level. ** Significant correlation ($0.6 < r_s < 1$) at the 0.01 level.

achieved *via* molecular titration of an orthogonal extracytoplasmic function (ECF) σ and anti-σ factor pair, with σ activating GFP expression.[15] The computation system shows predictive measurement of the two signal intensities with tunable and proportional GFP expression in response to a defined regime of combinations of the two signal concentrations. This system is a useful orthogonal module that can be used in pathway engineering for biotechnological and synthetic biology applications, in order to achieve complex programming of engineered cells.

The molecular titration system at the core of the computation module (Figure 1A) is composed of the orthogonal ECF20_992

DOI: 10.1021/acssynbio.7b00109
ACS Synth. Biol. XXXX, XXX, XXX–XXX

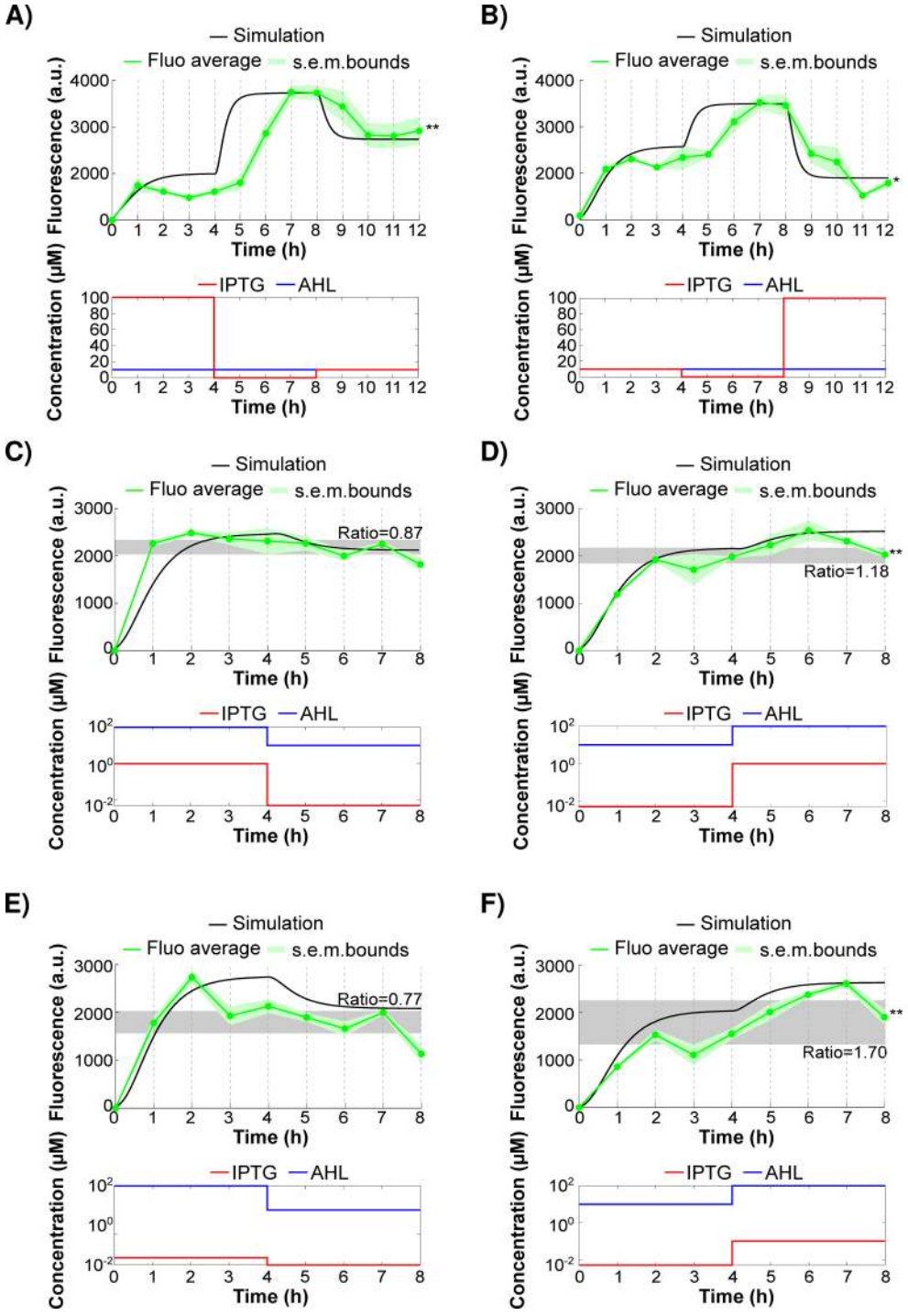

Figure 3. The computation module can be used to generate desired expression profiles. (A–F) Mathematical simulations (black lines) and measured GFP expression profile (green line) in the indicated combination of AHL and IPTG concentrations: (A–B) Square waves generation; (C–D) buffering ability; (E–F) unbuffered controls. GFP fluorescence was measured and cells diluted every hours (dashed gray lines). Data are averages of three independent experiments and s.e.m. is shown as shadowed green area. Spearman's correlation coefficient (r) and p-value (p): (A) $r_s = 0.804$; $p = 0.001$; (B) $r_s = 0.629$; $p = 0.021$; (C) $r_s = 0.433$; $p = 0.244$; (D) $r_s = 0.866$; $p = 0.003$; (E) $r_s = 0.260$; $p = 0.500$ (F) $r_s = 0.866$; $p = 0.003$. * Significant correlation ($0.6 < r_s < 1$) at the 0.05 level. ** Significant correlation ($0.6 < r_s < 1$) at the 0.01 level. (C–F) gray area indicates the region formed by the mean value between 3 h and 4 h and mean value between 7 h and 8 h. Fold increase of the latter with respect to the former is indicated as "ratio".

σ and anti-σ pair from *Pseudomonas fluorescens* Pf-5.[16] Its specificity and orthogonality in *E. coli* has previously been described.[15] The σ and anti-σ pair can be expressed in *E. coli* cells without affecting cell viability and growth, can regulate the expression of a GFP protein encoded by the specific σ promoter (p20_992), and has little crosstalk with native host components.

In our module the σ_20_992 gene is under the control of the AHL-responsive promoter plux, the anti-σ_20_992 gene is under the control of the IPTG-responsive promoter plac-UV5, and the sfGFP gene is under the control of the σ_20–992-responsive promoter, p20_992 (Table S1). All proteins were destabilized by promoting their proteolysis *via* an ssrA-tag, to

DOI: 10.1021/acssynbio.7b00109
ACS Synth. Biol. XXXX, XXX, XXX–XXX

ensure fast dynamic responses of expression.[17] In this way the computation function is achieved by the sequestration of the σ protein (activated by the AHL signal) by the anti-σ protein (activated by the IPTG signal) so that only the resulting free σ is able to trigger the expression of the GFP protein. Hence the relative intensity of the two signals (AHL and IPTG) is constantly computed and the GFP expression is proportionally adapted to their relative abundances.

A good computation system should have a defined regime of operation with good tunability and sensitivity. To test this we incubated transformed *E. coli* MG1655 cells with 84 different combinations of inducer concentrations, and measured GFP fluorescence after 3, 4, and 5 h (Figure 1B). The GFP fluorescence was coherently adapted to the computation output (difference between the AHL and the IPTG concentrations), with a defined range of concentrations (IPTG between 10 nM and 100 μM, AHL between 1 μM and 1 mM) (Figure 1B and Figure S1A). We argue that differences in the values observed at low IPTG concentrations are due to biological noise, rather than to a specific effect, as suggested by the s.e.m. values (Table S2). The system was able to reach steady-state regulation within 4 h, showing less than 20% of overall change between 3 h and 4 h and around 10% of overall change between 4 h and 5 h (Figure S1B), indicating that the system is already at steady-state at 4 h post-treatment. The signal computation function and the resulting tunability range is dependent on the σ/anti-σ system, as it was not observed in the absence of the anti-σ protein (Figure S2). To complement the experiments, we developed a mathematical model of 4 ODEs (details in Supporting Information) to describe the system behavior. We then used steady state fluorescence data (Figure 1B, 4 h), as described in Supplementary Section S4, to fit model parameters and simulated the observed experimental conditions (Figure 1C and Figure S3), showing that the model effectively captures most of the qualitative behavior detected during the experiments.

Next, we analyzed the dynamical response of the system by performing time course experiments in continuous batch cultures, where cells were constantly kept in exponential growth phase by diluting them every hour (dashed lines in Figure 2 and Figure 3) and challenging them with a fixed concentration of one signal and a 4 h step increasing or decreasing concentration of the other. When cells were challenged with a fixed concentration of 10 μM AHL and a time varying IPTG concentration (100, 50, 0 μM, Figure S4), we found that the decrease or increase in IPTG concentration resulted in a consistent increase or decrease of GFP expression levels (Figure 2A–B), measured at steady state after the 2–3 h transient response. Treatment with 10 μM AHL alone produced stable GFP expression, with only small variations from the mean value (Figure 2C). These experiments confirm that GFP levels are adapted to the computed relative amounts between the concentrations of IPTG and AHL and do not change when the IPTG signal is lacking.

We also confirmed the dynamic behavior of the system in experiments where cells were challenged with a fixed concentration of 50 μM IPTG and decreasing or increasing steps of AHL concentrations (0, 1, and 10 μM, Figure S4). GFP expression levels coherently adapted to the relative amounts of IPTG and AHL signals, after a transient response of 2–3 h (Figure 2D and F). As expected, the same GFP expression profile with higher maximal levels was reached in cells induced with the same AHL signal, but in the absence of IPTG (Figure 2E and G). This demonstrates that the response to one input can be tuned by the concentration of the other. We measured high correlation between the GFP expression profile and the comparator output (defined as the error measure between the reference [IPTG] and measured input [AHL]) in almost all of the conditions (Spearman's correlation coefficient between 0.7 and 0.9).

To qualitatively validate the fitting of the mathematical model (Figure 1C) we simulated the behavior of the system in the same experimental conditions (Figure 2A–G, black lines). Parameterization of the model is particularly challenging in this case as a single set of parameter values needs to be selected to capture both steady state experimental data and time lapses to two concurrent inputs. There is therefore an unavoidable trade-off to be made in order to carry out the multiobjective optimization strategy required for parameter selection. The parameter values we present were found *via* a combination of nonlinear optimization techniques and heuristics, and represent the best solution we found *via* an exhaustive numerical experiments campaign. The model was able to replicate most of the observed behavior, with the exception of the intermediate steady state levels in response to changes in AHL (Figure 2E–G), where the model was able to qualitatively capture the step increase or decrease in GFP expression but not the intensity of such changes. We believe this is likely due to the unavoidable compromises made during model parametrization and, possibly, unpredicted AHL internalization dynamics. Nevertheless, even in this case, the model predictions capture the overall trends of the GFP expression profiles observed in the experiments.

To determine the capability of the module to generate designed gene expression patterns, we tried (i) to program square wave outputs, and (ii) to maintain a fixed output level in the face of changes in one input signal by virtue of compensatory changes in the second. To test (i), we generated a square wave pattern, with different expression levels, by stimulating cells with a square wave IPTG signal (increasing or decreasing 100, 0, 10 μM, Figure S5A–B), and a fixed amount of 10 μM AHL signal in continuous batch cultures. The system took approximately 2 h to reach the different desired GFP expression levels (encoded by the combination of signal intensities and proportional to differences in their concentrations) after each input change (Figure 3A–B, green lines). To validate (ii), we predicted by using steady state data (Figure 1B, 4 h) that an increase from 10 μM AHL + 5 nM IPTG to 100 μM AHL would require an increase of IPTG to 10 μM in order to keep GFP expression constant. We tested the predictions in continuous batch culture, challenging cells for 4 h with the first inducer combination and then for an additional 4 h with the second inducer combination. We found that the GFP expression levels were kept constant both when moving from the higher to the lower combination of concentrations (Figure 3C and Figure S5C) and vice versa (Figure 3D and Figure S5D). As expected the buffering effect is not observed when the change in the IPTG concentration is calculated not to compensate for the change in AHL concentration (Figure 3E–F and Figure S5E–F; compare the dimension of the area formed by the mean value between 3 h and 4 h or 7 h and 8 h in Figure 3C–F). We measured high correlation between the GFP signal and the input in almost all of the conditions tested (Spearman's correlation coefficient between 0.7 and 0.9). We mathematically simulated the experimental observations (Figure 3A–F, black lines), finding that the model captures again the qualitative behavior observed experimentally, albeit with some mismatches in transient behavior.

An interesting application of the module we derived is the implementation of a negative feedback control scheme, where a

DOI: 10.1021/acssynbio.7b00109
ACS Synth. Biol. XXXX, XXX, XXX–XXX

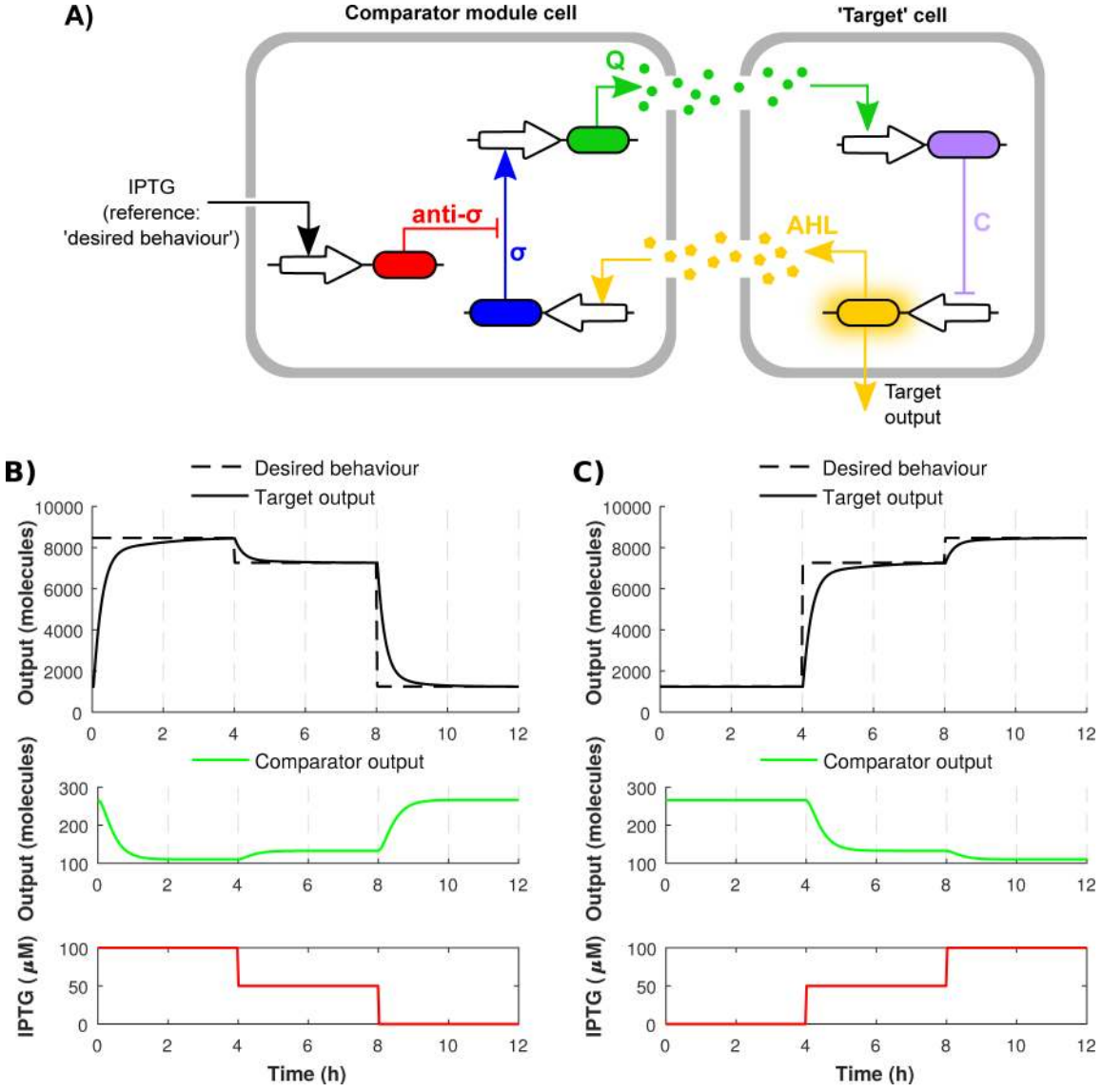

Figure 4. The computation module can be embedded in complex meta-devices. (A) A schematic illustration of a possible scheme coupling our computational module to a second cell population, designated the "Targets", to form a multicellular consortium designed to act as a distributed feedback controller. The objective is to control the target cells' output (yellow). The output expression is coupled to generation of AHL, which is sensed by the comparator cells allowing them to measure the effective output of the targets. The measured output is compared to an external IPTG concentration, which designates a desired temporal profile for the output of the targets, using our σ/anti-σ module. The result of this comparison is a measure of the difference between the desired reference and the actual output of the targets; this is coupled to the generation of an orthogonal quorum molecule designated Q (green), which is fed back to the targets. Finally, this feedback signal actuates a repression on the target GRN's output thus closing the control loop on the target output. (B) and (C) show *in silico* experiments validating the ability of our comparator module to function as expected in the proposed consortium. The desired multistep output is plotted in the top panels as a dashed line; the actual target output tracking this desired signal, as controlled by the computation module, is plotted as a solid black line. The central panel indicates the actual comparator output over time (green). Finally, the lower panel shows that actual IPTG reference signals corresponding to those in Figure 2A (B), and Figure 2B (C), that are fed to the comparator module to signal the desired response.

variable (*e.g.*, gene expression level) is constantly measured, compared to a desired level (the reference signal) in a process called reference-comparison, and adapted to the reference signal *via* an actuation module.[18,19] Such a scheme could be used for bioprocessing or biomedical applications, such as to improve the yield of metabolite production[20] or to program bacteria-based drug delivery in pathological conditions.[4] Currently a reference-comparison function has been achieved only *via* external *in silico* computation, requiring complex experimental set-ups.[19,21] As demonstrated in this paper, and recently proposed in theoretical work,[22] molecular titration is a good candidate to implement the reference computation function in a single population or a multicellular consortium.[23,24] To test and validate the use of our module in this context, we performed *in silico* experiments implementing the multicellular control strategy we recently presented[24] *via* the module described in this paper. Results shown in Figure 4 and Figure S6 confirm that the module, as modeled here, can effectively be integrated within a complex multicellular control scheme, whose in vivo validation is the subject of ongoing work.

In conclusion, we have designed, implemented and tested a biological computation module based on σ/anti-σ titration, able

DOI: 10.1021/acssynbio.7b00109
ACS Synth. Biol. XXXX, XXX, XXX−XXX

to dynamically integrate different concentrations of two signals and adapt its output to the computed signal. We have shown the full operation regime of the system, in biologically relevant concentrations of the two inducers, extending the analysis performed by Rhodius *et al.*[15] The system can process and compute, in experimentally useful time scales, multiple combinations of signal intensities and can be used to generate desired GFP expression patterns or to buffer sudden changes in one of the two signals. In some treatments we observed higher fluctuations around the mean expression values (Figure 2A−C and Figure 2F−G) possibly due to the complex experimental design and to intrinsic biological noise. We have derived and validated a mathematical model, parametrized on the experimental data. Parameter sensitivity analysis reported in Supporting Information, Figures S7, S8, was also carried out to show that the predicted model dynamics are robust to parameter perturbations. The parametrized model allows *in silico* testing of the use of this module in different applications, as for example the multicellular control strategy we validated above.

In addition to this, computing the difference between the amounts of two signals (biomarkers) is also of great interest to differentiate between physiologic and pathologic states, such as precancerous *versus* cancerous stage[25,26] or latent *versus* infective stage.[27] Our computation system could be used to detect a multiplexed "injury code" for a specific pathogenic condition and elicit a particular response (such as expression of repair metabolites or genes).

Our approach can be extended by using multiple σ/anti-σ pairs, processing different signals and linked to multiple expression modules, making it a powerful solution for different biotechnological applications. For example, there is great interest in biosensors for detection of environmental pollutants[28,29] or cancer and pathological biomarkers,[3,30] but all the proposed systems have a limited sensitivity range, which is generally determined by the promoter used for the detection of the desired signal. In all these cases, our system, in which a control signal tunes the region of responsiveness to a second signal can be of immediate application.

MATERIALS AND METHODS

Plasmids and Strains. *Escherichia coli* strain XL1-Blue (*recA1 endA1 gyrA96 thi-1 hsdR17 supE44 relA1 lac [F́ proAB lacI^{q}ZΔM15 Tn10 (Tet^r)]*) (from Stratagene, #200249) was used for all the cloning manipulations of this work.

Escherichia coli strain MG1655 (*λ-, rph-1*)[31] was used for all the assays in this work (Guyer *et al.*, 1981), and transformed with the three plasmids constituting the computation system, unless stated otherwise.

The computation system is composed of three plasmids: pLuSb (medium copy number), pVRa_LacASb_Flag (medium copy number) and pVRb_ssrA (low copy number). The genes constituting the essential core of the computation module (σ, anti-σ and GFP) are ssrA tagged (AANDENYALAA) to ensure fast dynamics of expression and degradation.

Vector backbones were derived from plasmids pVRa20_992, pVRb20_992 and pVRc20_992.[15]

The pLuSb plasmid (Table S1) encodes the LuxR gene, under the control of the lacI promoter, and the σ gene under the control of the plux promoter, and was built by standard restriction digestion and ligation cloning procedure. The 6xHis-Sigma-ssrA gene was amplified by the pVRa20_992 plasmid (from Addgene, #49673) with primers Sigma_FW and Sigma_ssrA_RW, and cloned NdeI/BamH1 in plasmid pVRc20_992 (from Addgene, #49739).

The pVRa_LacASb_Flag plasmid (Table S1) encodes the LacI gene, under the control of the lacI promoter, and the antisigma-ssrA-Flag gene, under the control of the lacUV5 promoter and was cloned in a two step cloning procedure. First the pBaASb plasmid was obtained by standard restriction digestion and ligation procedure, by amplifying the Anti-Sigma gene from the pVRc20_992 plasmid (Addgene #49739) with primers AntiSigma_FW and AntiSigma_ssrA_RW and cloning the PCR product in pBAD/His_iRFP plasmid (Addgene #31855) after NcoI/*Bam*HI digestion. Second the pVRa_LacASb plasmid was obtained by standard Gibson isothermal cloning technique: plasmid backbone was amplified from the pVRa20_992 plasmid with primers LacIASb_Vector_F and LacIASb_Vector_R; plac promoter was amplified from plasmid pSR/lacUV5[32] with primers LacIASb_Frag1_F and LacIASb_Frag1_R; anti-σ gene was amplified from pBaASb plasmid with primers LacIASb_Frag2_F and LacIASb_Frag2_R. In a second step the Flag tag was added to the pVRa_LacASb plasmid by rolling circle PCR amplification with primers ASb_Flag_F and ASb_Flag_R.

The pVRb_ssrA plasmid (Table S1) encodes the sfGFPssrA gene, under the control of the p20_992 promoter, and was built from the pVRb20_992 plasmid (from Addgene, #49714) by whole-plasmid PCR amplification and ligation with primers GFPssrA_F and GFPssrA_R.

Primer sequences are in Table S3.

Cells were transformed with standard $CaCl_2$ heat-shock transformation procedure and grown on LB-Agar plates with appropriate antibiotic selections.

All plasmid sequences were confirmed by sequencing service (Eurofins Genomics).

Reagents and Media. In all the assays and cloning manipulations cells were grown in Luria−Bertani Medium (from MP Biomedicals, #113002011).

AHL (3-oxo-*N*-(2-oxotetrahydro-3-furanyl) hexanamide from Key Organics, #MS2575) was dissolved in water, filter-sterilized and added to LB medium at the indicated concentrations.

IPTG (Isopropyl β-D-1-thiogalactopyranoside from Sigma-Aldrich, #I5502) was dissolved in water, filter-sterilized and added to LB medium at the indicated concentrations.

Antibiotic were used at the following working concentrations: Ampicillin (Sigma-Aldrich #A9518) 100 μg/μL, Kanamycin (Sigma-Aldrich #K4000) 50 μg/μL, Chloroamphenicol (Sigma-Aldrich #C0378) 25 μg/μL.

96-Well Fluorescence Assays. To perform steady state and wide range analysis of the computation module in 96 well plates, colonies from freshly transformed cells were grown for 12 h at 37 °C in a shaking incubator in 5 mL of LB medium and appropriate antibiotic selection. After 12 h cells were diluted 100 fold in 20 mL of prewarmed LB medium (with appropriate antibiotics), grown at 37 °C in a shaking incubator to an OD_{600} of 0.3 (approximately 2 h) and then 100 μL of the cell suspension was added to each well of a standard flat bottom 96-well plate, previously loaded with 100 μL of LB containing 2× the desired final inducer concentration, in a final volume of 200 μL of LB medium. Plates were incubated in a shaking mini-incubator (TECAN Freedom EVO II workstation) at 37 °C; at each time point GFP fluorescence (excitation 485 nm, emission 530 nm, cutoff 515 nm) and OD_{600} were measured with a TECAN Infinite M200 Pro plate reader.

DOI: 10.1021/acssynbio.7b00109
ACS Synth. Biol. XXXX, XXX, XXX−XXX

Background (LB medium) values were subtracted from GFP values and the resulting numbers were normalized on the OD_{600} measurements and the results from three independent experiments were averaged. Finally the normalized values within each time point were scaled across the full dynamical range (measured value − min value/(max value − min value)) and shown as heatmap.

Dynamical Fluorescence Quantification Assays. To perform dynamical characterization of the computation module in liquid cultures, colonies from freshly transformed cells were grown for 12 h at 37 °C in 5 mL of LB medium and appropriate antibiotic selection. After 12 h cells were diluted 100 fold in 5 mL of fresh LB medium (with appropriate antibiotics), grown at 37 °C in a shaking incubator to an OD_{600} of 0.3 (approximately 2 h) and then diluted 3 fold in 5 mL of prewarmed LB medium, with indicated concentrations of inducer molecules and appropriate antibiotics. Every hours 1 mL of samples was taken to measure OD_{600} and stored at 4 °C for subsequent GFP fluorescence analysis, while an appropriate amount of cell suspension was spun down (13200 rpm for 1 min) and suspended in 5 mL of prewarmed LB medium with the same concentration of inducers and antibiotics, in order to keep cell in logarithmic phase (OD_{600} between 0.3 and 0.6). When inducer concentrations were changed, cells were washed with 500 μL of PBS (137 mM NaCl, 2.7 mM KCl, 10 mM Na_2HPO_4, 1.8 mM KH_2PO_4, pH 7.4) before being suspended in prewarmed LB medium with the new inducers concentrations.

At the end of the time course 200 μL of each sample were loaded in a 96 well plate and GFP fluorescence measured (excitation 485 nm, emission 530 nm, cutoff 515 nm) in a FLEXstation (VWR) system. Background (LB medium) values were subtracted from GFP values and the resulting numbers were normalized on the OD_{600} measurements.

Statistical Analysis. For dynamic response experiments Spearman rank-order correlation coefficient[33] was calculated between the mean GFP intensity profile (from three independent experiments) and the computed signal (AHL-IPTG), by using the 2-tailed bivariate correlation option in IBM SPSS statistic software.

Mathematical Model. An Ordinary Differential Equation (ODE) model was derived considering all the key reactions of the system involving σ, anti-σ and their complex, as well as the measurable GFP. The final (simplified) model, consisting of 4 ODEs, was used for parameter identification, and subsequently for simulations of the steady-state behavior of the system as well as its temporal dynamics. Further details of model derivation and parametrization are provided in the Supporting Information.

***In Silico* Experiments of Multicellular Control Strategy.** The Ordinary Differential Equation (ODE) model of the module, defined and parametrized above, was embedded in the more complex model of a multicellular control strategy presented in Fiore *et al.*, 2017[24] and reported in Supporting Information, Section S5. Simulations were carried out in MATLAB.

■ ASSOCIATED CONTENT

Supporting Information

The Supporting Information is available free of charge on the ACS Publications website at DOI: 10.1021/acssynbio.7b00109.

Supplementary methods and implementation details; supporting details of case study; supporting figures (PDF)

■ AUTHOR INFORMATION

Corresponding Authors

*E-mail: m.dibernardo@bristol.ac.uk.
*E-mail: n.j.savery@bristol.ac.uk.

ORCID

Antoni Matyjaszkiewicz: 0000-0002-8647-5773
Gianfranco Fiore: 0000-0002-5713-5323
Nigel J. Savery: 0000-0002-0803-4075

Author Contributions

#F.A. and A.M. contributed equally. M.d.B. and N.J.S. contributed equally.

Notes

The authors declare no competing financial interest.

■ ACKNOWLEDGMENTS

We thank the BrisSynBio Biosuite facility and Dr. Peter Wilson for support with the 96-well fluorescence measurement experiments in the TECAN platform. This work was supported by BrisSynBio, a BBSRC/EPSRC Synthetic Biology Research Centre, grant number: BB/L01386X/1.

■ REFERENCES

(1) Levy, S., and Barkai, N. (2009) Coordination of gene expression with growth rate: a feedback or a feed-forward strategy? *FEBS Lett. 583*, 3974−3978.

(2) Tamari, Z., Rosin, D., Voichek, Y., and Barkai, N. (2014) Coordination of gene expression and growth-rate in natural populations of budding yeast. *PLoS One 9*, e88801.

(3) Danino, T., Prindle, A., Kwong, G. A., Skalak, M., Li, H., Allen, K., Hasty, J., and Bhatia, S. N. (2015) Programmable probiotics for detection of cancer in urine. *Sci. Transl. Med. 7*, 289ra284.

(4) Din, M. O., Danino, T., Prindle, A., Skalak, M., Selimkhanov, J., Allen, K., Julio, E., Atolia, E., Tsimring, L. S., Bhatia, S. N., and Hasty, J. (2016) Synchronized cycles of bacterial lysis for in vivo delivery. *Nature 536*, 81−85.

(5) Angelici, B., Mailand, E., Haefliger, B., and Benenson, Y. (2016) Synthetic Biology Platform for Sensing and Integrating Endogenous Transcriptional Inputs in Mammalian Cells. *Cell Rep. 16*, 2525−2537.

(6) Auslander, S., and Fussenegger, M. (2013) From gene switches to mammalian designer cells: present and future prospects. *Trends Biotechnol. 31*, 155−168.

(7) Benenson, Y. (2012) Biomolecular computing systems: principles, progress and potential. *Nat. Rev. Genet. 13*, 455−468.

(8) Didovyk, A., Kanakov, O. I., Ivanchenko, M. V., Hasty, J., Huerta, R., and Tsimring, L. (2015) Distributed classifier based on genetically engineered bacterial cell cultures. *ACS Synth. Biol. 4*, 72−82.

(9) Klauser, B., Saragliadis, A., Auslander, S., Wieland, M., Berthold, M. R., and Hartig, J. S. (2012) Post-transcriptional Boolean computation by combining aptazymes controlling mRNA translation initiation and tRNA activation. *Mol. BioSyst. 8*, 2242−2248.

(10) Nilgiriwala, K. S., Jimenez, J., Rivera, P. M., and Del Vecchio, D. (2015) Synthetic tunable amplifying buffer circuit in *E. coli*. *ACS Synth. Biol. 4*, 577−584.

(11) Tamsir, A., Tabor, J. J., and Voigt, C. A. (2011) Robust multicellular computing using genetically encoded NOR gates and chemical 'wires'. *Nature 469*, 212−215.

(12) Buchler, N. E., and Cross, F. R. (2009) Protein sequestration generates a flexible ultrasensitive response in a genetic network. *Mol. Syst. Biol. 5*, 272.

(13) Shopera, T., Henson, W. R., Ng, A., Lee, Y. J., Ng, K., and Moon, T. S. (2015) Robust, tunable genetic memory from protein sequestration combined with positive feedback. *Nucleic Acids Res. 43*, 9086−9094.

DOI: 10.1021/acssynbio.7b00109
ACS Synth. Biol. XXXX, XXX, XXX−XXX

(14) Hsiao, V., de los Santos, E. L. C., Whitaker, W. R., Dueber, J. E., and Murray, R. M. (2014) Design and implementation of a biomolecular concentration tracker. *ACS Synth. Biol. 4*, 150−161.
(15) Rhodius, V. A., Segall-Shapiro, T. H., Sharon, B. D., Ghodasara, A., Orlova, E., Tabakh, H., Burkhardt, D. H., Clancy, K., Peterson, T. C., Gross, C. A., and Voigt, C. A. (2013) Design of orthogonal genetic switches based on a crosstalk map of sigmas, anti-sigmas, and promoters. *Mol. Syst. Biol. 9*, 702.
(16) Staron, A., Sofia, H. J., Dietrich, S., Ulrich, L. E., Liesegang, H., and Mascher, T. (2009) The third pillar of bacterial signal transduction: classification of the extracytoplasmic function. (ECF) sigma factor protein family. *Mol. Microbiol. 74*, 557−581.
(17) Gottesman, S., Roche, E., Zhou, Y., and Sauer, R. T. (1998) The ClpXP and ClpAP proteases degrade proteins with carboxy-terminal peptide tails added by the SsrA-tagging system. *Genes Dev. 12*, 1338−1347.
(18) Fiore, G., Perrino, G., di Bernardo, M., and di Bernardo, D. (2016) In Vivo Real-Time Control of Gene Expression: A Comparative Analysis of Feedback Control Strategies in Yeast. *ACS Synth. Biol. 5*, 154−162.
(19) Menolascina, F., Fiore, G., Orabona, E., De Stefano, L., Ferry, M., Hasty, J., di Bernardo, M., and di Bernardo, D. (2014) In-vivo real-time control of protein expression from endogenous and synthetic gene networks. *PLoS Comput. Biol. 10*, e1003625.
(20) Dunlop, M. J., Keasling, J. D., and Mukhopadhyay, A. (2010) A model for improving microbial biofuel production using a synthetic feedback loop. *Syst. Synth Biol. 4*, 95−104.
(21) Milias-Argeitis, A., Summers, S., Stewart-Ornstein, J., Zuleta, I., Pincus, D., El-Samad, H., Khammash, M., and Lygeros, J. (2011) *in silico* feedback for in vivo regulation of a gene expression circuit. *Nat. Biotechnol. 29*, 1114−1116.
(22) Briat, C., Gupta, A., and Khammash, M. (2016) Antithetic Integral Feedback Ensures Robust Perfect Adaptation in Noisy Biomolecular Networks. *Cell Syst 2*, 15−26.
(23) Cuba Samaniego, C., Giordano, G., Kim, J., Blanchini, F., and Franco, E. (2016) Molecular Titration Promotes Oscillations and Bistability in Minimal Network Models with Monomeric Regulators. *ACS Synth. Biol. 5*, 321−333.
(24) Fiore, G., Matyjaszkiewicz, A., Annunziata, F., Grierson, C., Savery, N. J., Marucci, L., and di Bernardo, M. (2017) In-Silico Analysis and Implementation of a Multicellular Feedback Control Strategy in a Synthetic Bacterial Consortium. *ACS Synth. Biol. 6*, 507−517.
(25) Halamek, J., Windmiller, J. R., Zhou, J., Chuang, M. C., Santhosh, P., Strack, G., Arugula, M. A., Chinnapareddy, S., Bocharova, V., Wang, J., and Katz, E. (2010) Multiplexing of injury codes for the parallel operation of enzyme logic gates. *Analyst 135*, 2249−2259.
(26) Liu, Z., Sall, A., and Yang, D. (2008) MicroRNA: An emerging therapeutic target and intervention tool. *Int. J. Mol. Sci. 9*, 978−999.
(27) Latorre, I., and Dominguez, J. (2015) Dormancy antigens as biomarkers of latent tuberculosis infection. *EBioMedicine 2*, 790−791.
(28) Das, J., Sarkar, P., Panda, J., and Pal, P. (2014) Low-cost field test kits for arsenic detection in water. *J. Environ. Sci. Health, Part A: Toxic/Hazard. Subst. Environ. Eng. 49*, 108−115.
(29) Harms, H., Wells, M. C., and van der Meer, J. R. (2006) Whole-cell living biosensors–are they ready for environmental application? *Appl. Microbiol. Biotechnol. 70*, 273−280.
(30) Lai, Y. H., Sun, S. C., and Chuang, M. C. (2014) Biosensors with built-in biomolecular logic gates for practical applications. *Biosensors 4*, 273−300.
(31) Guyer, M. S., Reed, R. R., Steitz, J. A., and Low, K. B. (1981) Identification of a sex-factor-affinity site in *E. coli* as gamma delta. *Cold Spring Harbor Symp. Quant. Biol. 45*, 135−140.
(32) Savery, N. J., Lloyd, G. S., Kainz, M., Gaal, T., Ross, W., Ebright, R. H., Gourse, R. L., and Busby, S. J. W. (1998) Transcription activation at Class II CRP-dependent promoters: identification of determinants in the C-terminal domain of the RNA polymerase alpha subunit. *EMBO J. 17*, 3439−3447.
(33) Spearman, C. (1987) The proof and measurement of association between two things. By C. Spearman, 1904. *Am. J. Psychol. 100*, 441−471.

DOI: 10.1021/acssynbio.7b00109
ACS Synth. Biol. XXXX, XXX, XXX−XXX